Inorganic Chemistry

Article

pubs.acs.org/IC

Metal Chelation-Assisted Amine−Amine Electronic Coupling through the 4,4′-Positions of 2,2′-Bipyridine

Hai-Jing Nie, Wen-Wen Yang, Ren-Hui Zheng, Qiang Shi, Hui Chen, Jiannian Yao, and Yu-Wu Zhong*

Beijing National Laboratory for Molecular Sciences, CAS Key Laboratory of Photochemistry, State Key Laboratory for Structural Chemistry of Unstable and Stable Species, Institute of Chemistry, Chinese Academy of Sciences, 2 Bei Yi Jie, Zhong Guan Cun, Beijing 100190, People's Republic of China

Supporting Information

ABSTRACT: A redox-active diamine ligand, 4,4′-bis(di-*p*-anisylamino)-2,2′-bipyridine (NNbpy), has been prepared. Electrochemical and spectroscopic studies suggest that little electronic coupling is present between two amine groups in NNbpy. After chelation with $Ru(bpy)_2$ (bpy is 2,2′-bipyridine), the resulting complex displays two $N^{\bullet+/0}$ processes at +1.02 and +1.16 V versus Ag/AgCl. In the mixed-valent state, rich near-infrared absorptions have been observed, which are believed to consist of multiple metal-to-ligand charge transfer and intervalence charge transfer transitions in the low-energy region. These results suggest that the amine−amine electronic coupling has been enhanced by chelation with $Ru(bpy)_2$. In contrast, no efficient electronic coupling can be realized by chelation with $Ir(ppy)_2$ (ppy is 2′-phenylpyridine) or $Re(CO)_3Cl$. A ruthenium ion-mediated electron transfer mechanism, instead of through-space coupling, has been proposed to explain this phenomenon. For the purpose of comparison, a monoamine-substituted bpy ligand and corresponding $Ru(bpy)_2$ complex have been synthesized and studied. In addition, EPR, DFT, and TDDFT studies have been performed to complement the experimental results.

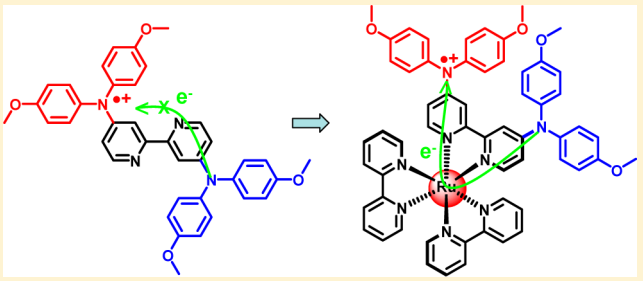

INTRODUCTION

Electron transfer (ET) is ubiquitous in nature and electronic devices. Since the invention of the Creutz-Taube ion,[1] mixed-valence (MV) chemistry has become a powerful means to examine the fundamental ET process among redox-active components.[2] Important ET parameters, such as reorganization energy and electronic coupling parameter, can be derived by intervalence charge-transfer (IVCT) analysis.[3]The studies of MV compounds are not only relevant to the understanding of the ET processes in nature, but also able to produce redox-active materials for various optoelectronic applications such as electrochromic devices,[4] molecular switches,[5] molecule electronics,[6] and information storage.[7]

The most common MV compound can be represented by the general formula, $[M_a^{\,n}-BL-M_b^{\,n+1}]$, where BL is an organic bridging ligand and M_a and M_b are redox-active inorganic or organometallic components, such as ferrocene[8] and ruthenium complexes.[9] In recent years, the use of purely organic species as the redox sites in MV chemistry has also received increasing attention,[10] including dihydrazines,[11] triarylamines,[12] quinones,[13] and nitrobenzene derivatives,[14] among others. In general, the BL in these organic MV systems is also made of a conjugated organic unit. However, a conceptually reverse system, consisting of organic redox sites bridged by an organometallic bridge, has remained rather unexplored.[15] Such a system is useful in estimating the strength of organometallic molecular wires[6] to mediate the electronic coupling between distal redox sites. In addition, consecutive multiple redox processes can be expected from these compounds, which will make them appealing for applications in molecular electronics.[16]

We present herein the amine−amine electronic coupling studies through the 4,4′-positions of 2,2′-bipyridine (bpy). We are particularly interested to know whether the electronic coupling in the bpy ligand **1** with two redox-active di-*p*-anisylamino substituents (NNbpy, Scheme 1) could be enhanced by metal chelation, e.g., with a $Ru(bpy)_2$ component. The $N^{\bullet+/0}$ potential for the chemically reversible oxidation of the di-*p*-anisylamino group substituted on tris-bipyridine or bis-terpyridine ruthenium complexes is known to be much less positive with respect to the $Ru^{III/II}$ potential.[15,17] The $Ru(bpy)_3$ core can be considered as an organometallic bridge to mediate the amine−amine coupling. If the amine−amine coupling can indeed be enhanced by metal chelation with $Ru(bpy)_2$, then another question arises. Does the amine−amine electronic coupling take place via a through-bond or through-space mechanism? In other words, we are interested to know if the metal ion species makes a difference to the electronic coupling. After metal chelation, the two di-*p*-anisylamino groups on each bpy ligand are in close proximity, and a through-space electronic coupling can be assumed. To address these questions, ruthenium complex **2**$(PF_6)_2$, iridium complex **3**(PF_6), and rhenium complex **4** with the NNbpy ligand and ruthenium

Received: August 12, 2014
Published: January 27, 2015

DOI: 10.1021/ic5024967
Inorg. Chem. 2015, 54, 1272−1282

Scheme 1. Synthesis of Compounds Studied in This Paper[a]

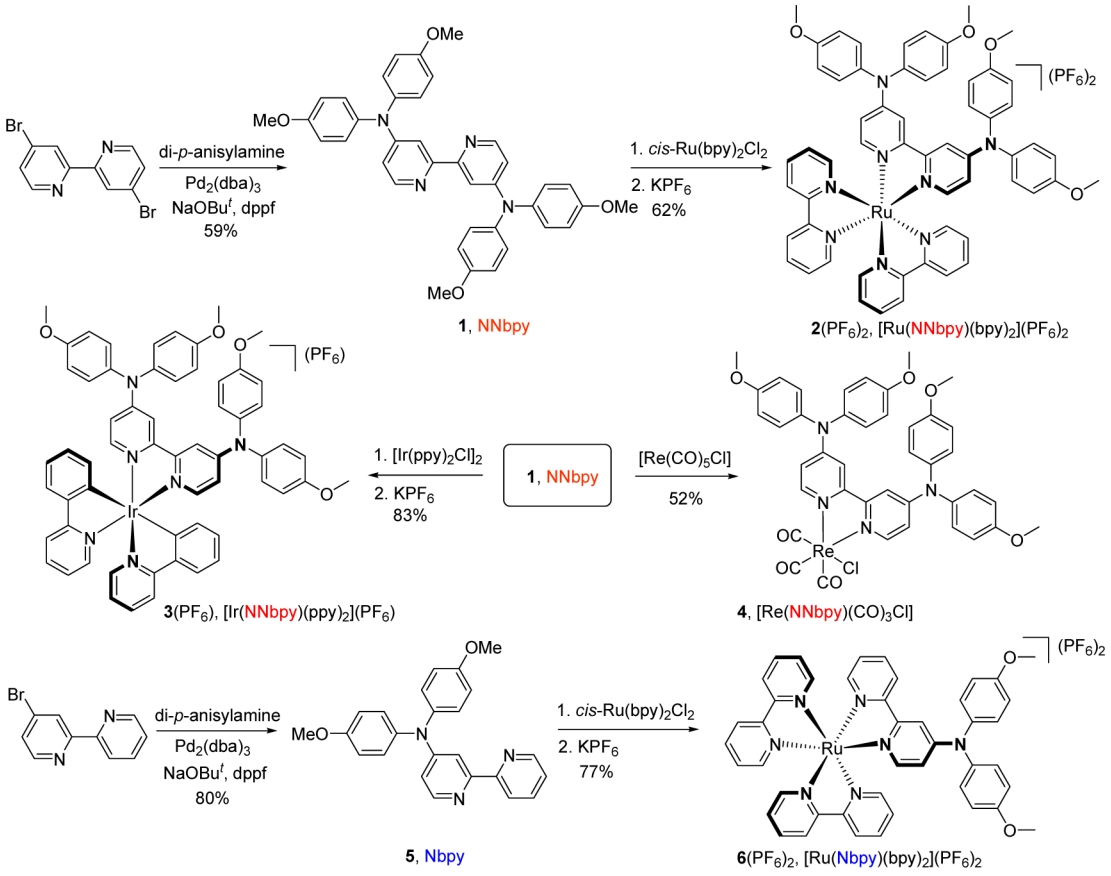

[a]bpy = 2,2′-bipyridine; ppy = 2-phenylpyridine.

complex $\mathbf{6}(PF_6)_2$ with one amine substituent have been synthesized (Scheme 1). These complexes have been studied by combined experimental and computational techniques, including electrochemical and near-infrared (NIR) spectral analysis, electron paramagnetic resonance (EPR) analysis, and density functional theory (DFT) and time-dependent DFT (TDDFT) calculations.

RESULTS AND DISCUSSION

Synthesis and Characterization. As outlined in Scheme 1, ligands **1** (NNbpy) and **5** (Nbpy) with two or one di-*p*-anisylamino substituents were synthesized via the palladium catalyzed C−N coupling between di-*p*-anisylamine with 4,4′-dibromo-2,2′-bipyridine or 4-bromo-2,2′-bipyridine[18] in 59% and 80% yield, respectively. The reaction of **1** with *cis*-$[Ru(bpy)_2Cl_2]$, followed by anion exchange using KPF_6, gave complex $\mathbf{2}(PF_6)_2$ in 62% yield. The iridium complex $\mathbf{3}(PF_6)$ and rhenium complex **4** were synthesized from the reaction of **1** with $[Ir(ppy)_2Cl]_2$ (ppy = 2-phenylpyridine) and $Re(CO)_5Cl$, respectively. The ruthenium complex $\mathbf{6}(PF_6)_2$ with one amine substituent was obtained from the reaction of ligand **5** with *cis*-$[Ru(bpy)_2Cl_2]$ in 77% yield.

The synthesis details are provided in the Experimental Section. New compounds have been characterized by NMR, mass spectrum, and microanalysis. Signals consistent with the chemical structures of above complexes, after losses of one or two PF_6^- anions (except the neutral rhenium complex **4**), are evidenced in their MALDI-TOF mass spectra.

It should be mentioned that hybrid materials composed of polypyridine metal complexes and redox-active amine motifs are known to possess intriguing electronic properties.[19] These complexes exhibit enhanced light absorption and are particularly useful for solar cell applications. However, few studies focus on the uses of these organometallic components as bridging units to mediate electronic coupling.

Electrochemical Studies. The electronic coupling in these complexes was first studied by electrochemical analysis (Figures 1 and 2 and Table 1). The cyclic voltammogram (CV) of the diamine ligand **1** shows one redox couple at +1.14 and an irreversible oxidation wave at +1.45 V versus Ag/AgCl with the conventional Bu_4NClO_4 electrolyte (Figure 1a). The differential pulse voltammogram (DPV) confirms the same result. The first redox couple, with a peak-to-peak potential separation (ΔE_p) of 94 mV, should be the result of the oxidations of two amine substituents, namely two overlapping $N^{\bullet+/0}$ processes. This suggests that, if the amine−amine electronic coupling is present in the free ligand NNbpy (**1**), the degree of coupling would be rather small. This is also supported by the following spectroelectrochemical measurements. The large peak-to-peak potential separation is partially caused by the relatively slow electron transfer kinetics under the measurement conditions. Note that the $N^{\bullet+/0}$ wave of the monoamine ligand **5** has a similar ΔE_p value (see below). The irreversible oxidation peak of **1** at +1.45 V is assigned to the further oxidation of the *in situ* generated $N^{\bullet+}$ species ($N^{2+/\bullet+}$ process), as has been observed in many triarylamine derivatives.[15,20] This irreversible oxidation peak is also evident on the CVs and DPVs of other complexes studied in this Article. Oxidative dimerization has been reported for triarylamine compounds.[20] However, the dimerization reaction

DOI: 10.1021/ic5024967
Inorg. Chem. 2015, 54, 1272−1282

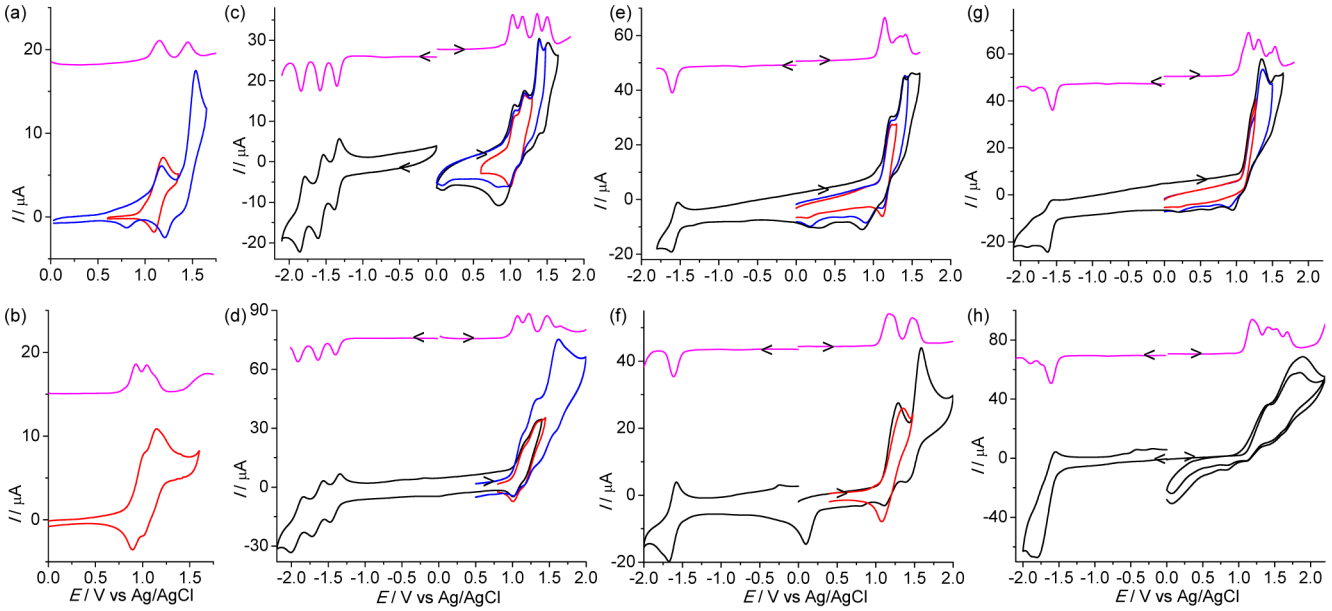

Figure 1. CVs of (a, b) **1**, (c, d) **2**$(PF_6)_2$, (e, f) **3**(PF_6), and (g, h) **4** with (a, c, e, g) Bu_4NClO_4 electrolyte or (b, d, f, h) $Bu_4NB(C_6F_5)_4$ electrolyte in CH_2Cl_2 at 100 mV/s at a glassy carbon electrode. The red curves show the $N^{\bullet+/0}$ processes of each compound. The insets show the DPV curves in magenta. Arrows indicate the initial direction of the potential scan.

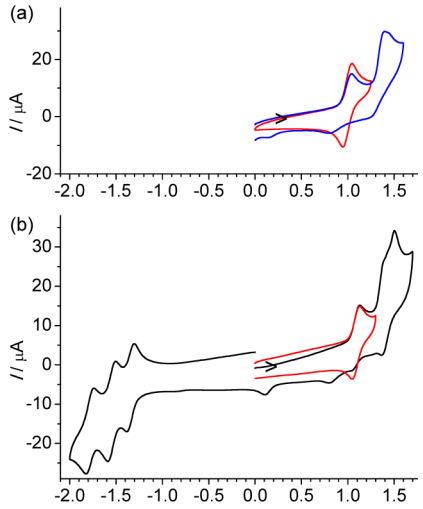

Figure 2. CVs of (a) **5** and (b) **6**$(PF_6)_2$ in CH_2Cl_2 at a glassy carbon electrode.

often takes place on the *para* position of the amine atom. The possibility of dimerization of **1** (also **5**) should be low because the *para* position is substituted with the methoxy group. When electrolyte $Bu_4NB(C_6F_5)_4$ with the weakly coordinating anion was used in the electrochemical measurement, the $N^{\bullet+/0}$ processes of **1** split into two waves with a potential separation of 115 mV (Figure 1b). However, no IVCT has been observed for **1** during the later spectroelectrochemical measurements with this electrolyte. The potential splitting is likely caused by Coulombic repulsion.

In stark contrast, when the NNbpy ligand was chelated to the ruthenium ion to form complex **2**$(PF_6)_2$, it displays two well-separated and chemically reversible $N^{\bullet+/0}$ processes at +1.02 and +1.16 V with Bu_4NClO_4 electrolyte (Figure 1c), with a potential splitting (ΔE) of 140 mV. This suggests that the amine−amine electronic coupling is enhanced by ruthenium chelation. This assertion will be further supported by the IVCT analysis discussed below. The comproportionation constant K_c for the equilibrium [N−N] + [$N^{\bullet+}$−$N^{\bullet+}$] → 2[N−$N^{\bullet+}$] is estimated to be 240 for the MV state, $\mathbf{2}^{3+}$. When $Bu_4NB(C_6F_5)_4$ electrolyte was used, the potential splitting of two $N^{\bullet+/0}$ processes becomes slightly bigger (155 mV, Figure 1d).

The redox couple at +1.48 V of **2**$(PF_6)_2$ should be assigned to the $Ru^{III/II}$ process, which is more positive with respect to that of $[Ru(bpy)_3](PF_6)_2$ (+1.35 V, Figure S1 in the Supporting Information). This is reasonable because the oxidized aminium cation motifs in the former complex behave as electron-deficient substituents and make the ruthenium component more difficult to be oxidized. In the cathodic scan of **2**$(PF_6)_2$, three bpy-associated reduction waves ($bpy^{0/-}$) are observed. The number of electrons for each $N^{\bullet+/0}$ process is proven by comparison with each $bpy^{0/-}$ process as an internal standard, which is a well-established one-electron process.

The ruthenium complex **2**$(PF_6)_2$ shows two well-separated $N^{\bullet+/0}$ processes. However, the situation is different for the iridium complex **3**(PF_6) and rhenium complex **4** (Figure 1e−h). Complex **3**(PF_6) shows a two-electron $N^{\bullet+/0}$ wave at +1.17 V (Figure 1e). Indeed, two close redox waves can be distinguished with $Bu_4NB(C_6F_5)_4$ electrolyte at this potential (Figure 1f). Again, the numbers of electron of the $N^{\bullet+/0}$ processes can be proven by comparison with the $bpy^{0/-}$ internal standard. For complex **4**, all anodic waves are severely irreversible, in the presence of either Bu_4NClO_4 or $Bu_4NB(C_6F_5)_4$ electrolyte (Figure 1g,h). The first oxidation peak at +1.20 V in Figure 1g can be assigned to the $N^{\bullet+/0}$ process, and the second peak at +1.36 V is assigned to the further irreversible oxidation of the aminium radical cation. The redox couples at +1.51 V of **3**(PF_6) and +1.53 V of **4** are very likely associated with the $Ir^{IV/III}$ and $Re^{II/I}$ processes,[21] respectively. However, because these processes occur after and overlap more or less with the irreversible $N^{2+/\bullet+}$ peak, it makes little sense to give more accurate assignments.

The monoamine ligand, Nbpy (**5**), shows a $N^{\bullet+/0}$ redox couple at +0.99 V and an irreversible $N^{2+/\bullet+}$ peak at +1.40 V (Figure 2a). The corresponding ruthenium complex **6**$(PF_6)_2$ displays a $N^{\bullet+/0}$

DOI: 10.1021/ic5024967
Inorg. Chem. 2015, 54, 1272−1282

Table 1. Electrochemical Data[a]

compd	anodic $E_{1/2}$[a] (ΔE_p/mV) amine-based	anodic $E_{1/2}$[a] (ΔE_p/mV) metal-based	cathodic $E_{1/2}$[a] (ΔE_p/mV)	$\Delta E_{echem,gap}$[b] (eV)
1, NNbpy	+1.14 (94, 2e), +1.45[c]			
2$(PF_6)_2$, $[Ru(NNbpy)(bpy)_2](PF_6)_2$	+1.02 (60), +1.16 (60), +1.35[c]	+1.48	−1.35 (68), −1.57 (70), −1.83 (68)	2.37
3(PF_6), $[Ir(NNbpy)(ppy)_2](PF_6)$	+1.17 (105, 2e), +1.40[c]	+1.51	−1.57 (72)	2.74
4, $[Re(NNbpy)(CO)_3Cl]$	+1.20 (2e), +1.36[c]	+1.53	−1.60 (60)	2.80
5, Nbpy	+0.99 (94), +1.40[c]			
6$(PF_6)_2$, $[Ru(Nbpy)(bpy)_2](PF_6)_2$	+1.08 (70), +1.38[c]	+1.44	−1.34 (74), −1.53 (74), −1.77 (77)	2.42
$[Ru(bpy)_3](PF_6)_2$		+1.35	−1.32, −1.52, −1.76	2.67

[a]Data with Bu_4NClO_4 electrolyte. The electrochemical potential is reported as the $E_{1/2}$ value vs Ag/AgCl unless otherwise noted. Potential versus ferrocene$^{+/0}$ can be estimated by subtracting 0.45 V. ΔE_p refers to the difference between the anodic and cathodic peak potential. [b]$\Delta E_{echem,gap}$, the electrochemical energy gap, is determined by the potential difference between the first anodic and cathodic redox wave. [c]Irreversible oxidation of $N^{\bullet+}$, E_{anodic}.

and $Ru^{III/II}$ redox couple at +1.08 and +1.44 V, respectively (Figure 2b).

The electrochemical energy gap ($\Delta E_{echem,gap}$), determined by the potential difference between the first oxidation and first reduction redox wave, is 2.37, 2.42, and 2.67 eV for **2**$(PF_6)_2$, **6**$(PF_6)_2$, and $[Ru(bpy)_3](PF_6)_2$, respectively. There is a clear trend that the presence of more amine substituents decreases the $\Delta E_{echem,gap}$ value in ruthenium complexes. In comparison, the $\Delta E_{echem,gap}$ values of the iridium complex **3**(PF_6) and the rhenium complex **4** (2.74 and 2.80 eV, respectively) are larger relative to those of the ruthenium complexes.

Spectroscopic Studies. The electronic absorption spectra of the above complexes are displayed in Figure 3. The absorption

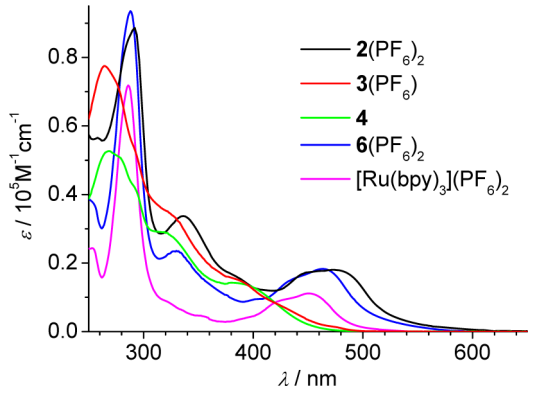

Figure 3. UV−vis absorption spectra in CH_2Cl_2.

maxima and molar extinction data are summarized in Table 2. All ruthenium complexes show intense absorption bands in the visible region, which are largely assigned to the metal-to-ligand charge-transfer (MLCT) transitions. However, for those containing amine substituents, the involvement of intraligand charge-transfer (ILCT) transitions and ligand-to-ligand charge-transfer (LLCT) is possible. This will be discussed later with the aid of the TDDFT results of $\mathbf{2}^{2+}$.

The absorption maxima in the visible region of **2**$(PF_6)_2$ and **6**$(PF_6)_2$ are 478 and 465 nm, respectively. Compared to that of $[Ru(bpy)_3](PF_6)_2$ ($\lambda_{abs,max}$ = 455 nm), the visible absorption of these amine-containing complexes exhibit a distinct red shift. With increasing number of the amine substituents, a descending order of the optical energy gap is present from $[Ru(bpy)_3](PF_6)_2$ to **6**$(PF_6)_2$ and **2**$(PF_6)_2$. This result is in agreement with the above electrochemical results. The iridium complex **3**(PF_6) and rhenium complex **4** do not show a well-separated visible

Table 2. Absorption Data in CH_2Cl_2[a]

	$\lambda_{abs,max}$ [nm] (ε/10^5 M^{-1} cm^{-1})
1	274(0.50), 312(0.27)
$\mathbf{1}^{2+}$	815 (0.063)
$\mathbf{2}^{2+}$	336(0.34), 382(0.16), 448(0.17), 478(0.18)
$\mathbf{2}^{3+}$	459 (0.17), 845 (0.16), 1620 (0.12)
$\mathbf{2}^{4+}$	495 (0.17), 870 (0.51), 1164 (0.14)
$\mathbf{3}^{+}$	264(0.78), 329(0.34), 387(0.15)
$\mathbf{3}^{3+}$	371 (0.24), 435 (0.14), 883 (0.42)
4	269(0.53), 325(0.28), 395(0.14)
$\mathbf{4}^{2+}$	462 (0.17), 893 (0.44)
5	230 (0.40)
$\mathbf{6}^{2+}$	288(0.93), 329(0.24), 435(0.15), 465(0.18)
$\mathbf{6}^{3+}$	414 (0.16), 846 (0.24), 1370 (0.10)
$[Ru(bpy)_3](PF_6)_2$	354 (0.051), 420 (0.087), 455 (0.11)

[a]The original counter-anions are PF_6^- as shown in Scheme 1, if present. $\mathbf{1}^{2+}$ was obtained by electrolysis, where counteranion ClO_4^- was introduced from the electrolyte. Other higher oxidation forms were obtained by chemical oxidation using $SbCl_5$, where counteranions $SbCl_6^-$ are included.

absorption band. Corresponding MLCT bands appear as shoulder absorptions around 400 nm, as has been observed in known bpy-containing iridium and rhenium complexes.[21] Compared to ruthenium complexes, the iridium and rhenium complexes show consistent bigger optical and electrochemical energy gaps.

In order to further examine the amine−amine electronic coupling of above compounds, they were stepwisely oxidized by electrolysis or chemical oxidation using $SbCl_5$ in CH_2Cl_2. Figure 4 shows the absorption spectral changes of the diamine ligand **1** upon gradually applying a potential from +0.8 to +1.4 V versus Ag/AgCl at an indium−tin−oxide (ITO) glass electrode, in the presence of either Bu_4NClO_4 or $Bu_4NB(C_6F_5)_4$ electrolyte. During this process, the ILCT absorption band at 312 nm decreased a little, and a distinct band at 815 nm appeared. The latter band is characteristic of the generation of aminium radical cations from neutral triarylamines.[12,15,20] In the NIR region, no IVCT absorption appeared at all during this oxidation process with both electrolytes (see the enlarged plot of the NIR absorptions in the inset of Figure 4). This suggests that little amine−amine electronic coupling is present in NNbpy **1**, consistent with the above electrochemical results. $SbCl_5$ is often used as the chemical oxidant to oxidize neutral triarylamines in MV studies.[12,15] However, it should be inappropriate for the oxidation of **1** due to the possible complexation of $SbCl_5$ to the free coordinating sites of bpy. For the remaining metal complexes, the

DOI: 10.1021/ic5024967
Inorg. Chem. 2015, 54, 1272−1282

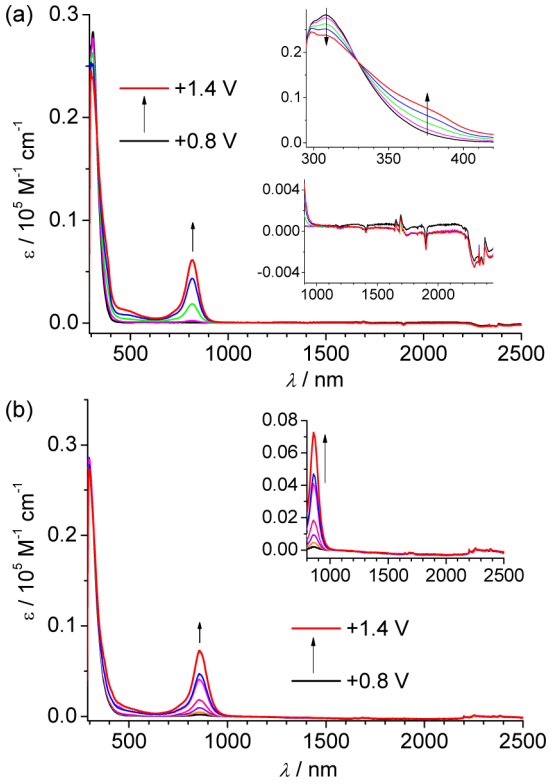

Figure 4. Absorption spectral changes of **1** (a) with Bu_4NClO_4 electrolyte and (b) with $Bu_4NB(C_6F_5)_4$ electrolyte in CH_2Cl_2 upon oxidative electrolysis from +0.8 to +1.4 V vs Ag/AgCl at an ITO glass surface. The inset shows the enlarged spectral changes in the UV and NIR region.

use of $SbCl_5$ as the chemical oxidant should be suitable. The $N^{\bullet+/0}$ potential of complexes **3**(PF_6) and **4** is quite high (around +1.20 V vs Ag/AgCl), and it proved difficult to completely oxidize the amine units of these two complexes by electrolysis. In this sense, chemical oxidation provides an alternative to probe the spectral changes upon stepwise oxidations.

When the ruthenium complex **2**$(PF_6)_2$ with one NNbpy ligand was subjected to the stepwise oxidation with $SbCl_5$ in CH_2Cl_2, two intense absorption bands at 845 and 1620 nm with a low-energy tail appeared at the single oxidation step with 1 equiv of $SbCl_5$ (Figure 5a). During the double oxidation step, the peak at 845 nm continued to increase and shifted slightly to 870 nm (Figure 5b). The NIR band at 1620 nm decreased significantly, with the concomitant appearance of a new band at 1164 nm. The intense peak at 845 nm of $\mathbf{2}^{3+}$ (and 870 nm of $\mathbf{2}^{4+}$) is clearly attributed to the $N^{\bullet+}$-localized transition. The character of the NIR band in the MV state will be discussed below. The new band at 1164 nm of $\mathbf{2}^{4+}$ is assigned to the MLCT transition from the ruthenium ion to the oxidized aminium unit, which will be further discussed below. Similar absorption spectral changes have been observed during the spectroelectrochemical measurements (Figure 5c–f), in the presence of either Bu_4NClO_4 or $Bu_4NB(C_6F_5)_4$ electrolyte. However, in the double oxidation step, the $N^{\bullet+}$-localized transition and the MLCT transition are much weaker with respect to those observed during chemical oxidation. This difference could be caused by the different anions used in these measurements or the slow oxidation kinetics due to a diffusion issue in electrolysis. In addition, the presence of electrolyte decreases the solubility of the oxidized species, which may also suppress the complete oxidation of the amine compounds. The spectral changes in Figure 5c,d are reversible when the oxidized complex was reduced back to the original state.

Figure 6a,b,d shows the absorption spectral changes of the Nbpy-containing ruthenium complex **6**$(PF_6)_2$ and the NNbpy-containing iridium complex **3**(PF_6) and rhenium complex **4** upon stepwise oxidation with $SbCl_5$, respectively. When **6**$(PF_6)_2$ was transformed into $\mathbf{6}^{3+}$, the appearance of the $N^{\bullet+}$-localized transition at 846 nm and the ruthenium → aminium MLCT

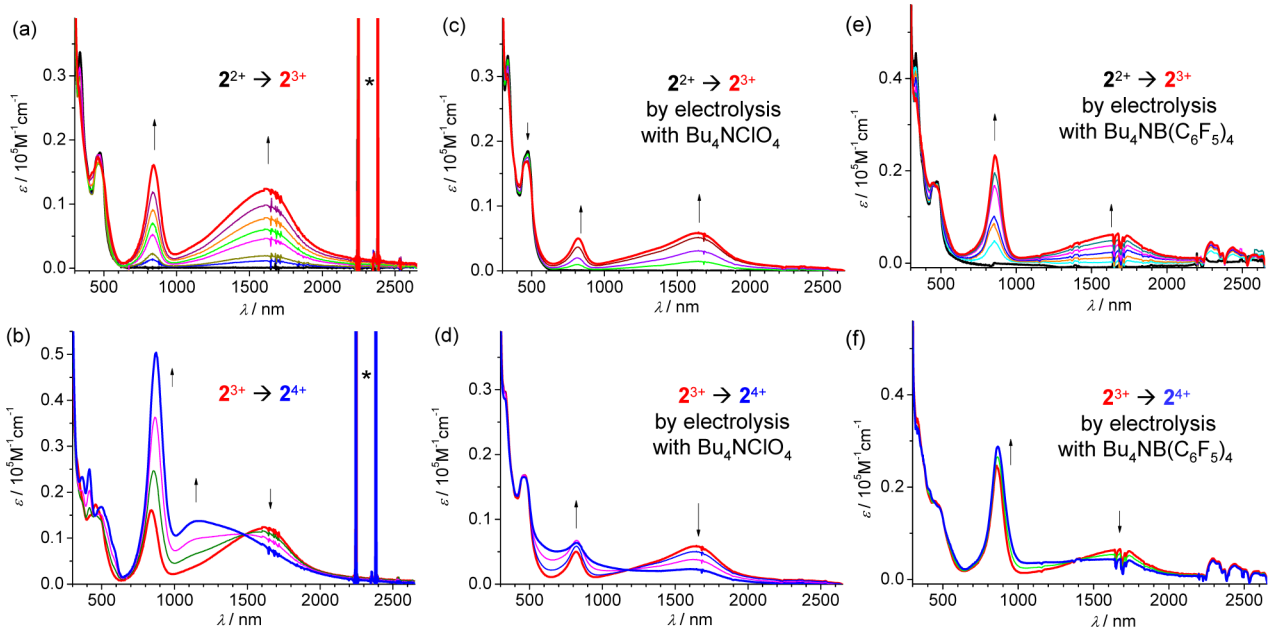

Figure 5. Absorption spectral changes of **2**$(PF_6)_2$ in CH_2Cl_2 upon (a, b) single and double oxidation using $SbCl_5$, (c, d) single (from +0.8 to +1.1 V) and double oxidation (from +1.1 to +1.35 V) by electrolysis in the presence of Bu_4NClO_4 electrolyte, and (e, f) single (from +0.8 to +1.1 V) and double oxidation (from +1.1 to +1.4 V) by electrolysis in the presence of $Bu_4NB(C_6F_5)_4$ electrolyte at an ITO glass surface. The applied potential was referenced versus Ag/AgCl. *: artifacts.

DOI: 10.1021/ic5024967
Inorg. Chem. 2015, 54, 1272–1282

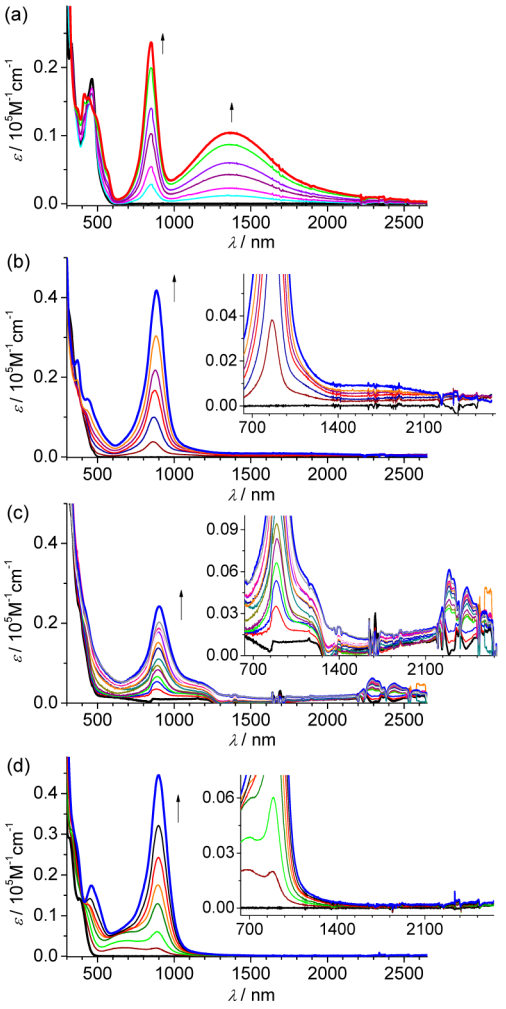

Figure 6. Absorption spectral changes of (a) $\mathbf{6}(PF_6)_2$, (b, c) $\mathbf{3}(PF_6)$, and (d) **4** in CH_2Cl_2 upon stepwise oxidation using $SbCl_5$ (for a, b, d) or by electrolysis in the presence of $Bu_4NB(C_6F_5)_4$ electrolyte (for c). The insets in parts b, c, and d show the enlarged plots in the NIR region.

transition at 1370 nm were observed (Figure 6a). For complexes $\mathbf{3}(PF_6)$ and **4**, only the appearance of the $N^{\bullet+}$-localized transitions around 900 nm was observed (Figure 6b,d). No possible IVCT band could be observed for these two complexes. This is also proven by the spectroelectrochemical measurements of $\mathbf{3}(PF_6)$ in the presence of the $Bu_4NB(C_6F_5)_4$ electrolyte (Figure 6c). Very weak NIR absorptions can be observed for complex $\mathbf{3}(PF_6)$ after oxidation, which are possibly a result of the iridium → aminium MLCT transitions. This band is initially invisible in the single oxidation of $\mathbf{3}(PF_6)$. It appears in the later stage of the double oxidation. It is unreasonable to assign this band to an IVCT transition. In the case of complex $\mathbf{4}^+$, the rhenium → aminium MLCT band might be shifted to the shoulder band around 650 nm. These results suggest that the N−N electronic coupling in NNbpy after metal chelation with $Ir(ppy)_2$ and $Re(CO_3)Cl$ is negligible, consistent with previous electrochemical results.

The above spectroscopic studies of $\mathbf{2}(PF_6)_2$ show that the NIR band at 1620 nm of $\mathbf{2}^{3+}$ significantly decreased upon further oxidation; this band is possibly due to the IVCT transitions of the MV state. However, the later TDDFT calculations of $\mathbf{2}^{3+}$ suggest that the absorptions in this region are largely due to the ruthenium → aminium MLCT transitions. The IVCT transition is predicted to locate at a lower-energy region with very weak oscillator strength. The asymmetric NIR band of $\mathbf{2}^{3+}$ obtained by chemical oxidation is fitted to four Gaussian functions (Figure 7),

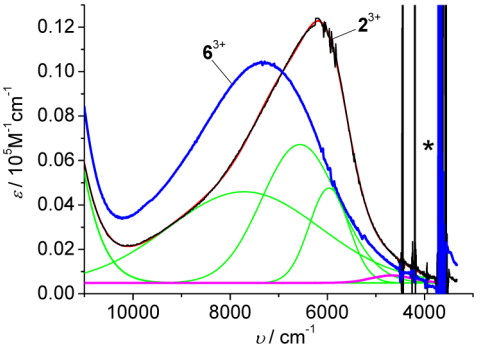

Figure 7. Gaussian-fitting of the NIR spectrum of $\mathbf{2}^{3+}$ obtained by chemical oxidation. Black curve is the experimental data. Red curve is the sum of the deconvoluted subbands. The magenta curve is the possible IVCT transition of $\mathbf{2}^{3+}$. The absorption spectrum of $\mathbf{6}^{3+}$ (blue curve) was included for comparison. *: artifacts.

where three subbands at 7730, 6560, and 5970 cm^{-1} (green curves) are responsible for the main absorptions and the weak band at 4670 cm^{-1} (magenta curve) is responsible for the low-energy tail absorptions. In comparison, the low-energy absorptions of $\mathbf{2}^{3+}$ are slightly red-shifted with respect to those of $\mathbf{6}^{3+}$. In accordance with the TDDFT results shown below, the weak subband at 4670 cm^{-1} is thus assigned to the potential IVCT transition. The electronic coupling parameter H_{ab} of $\mathbf{2}^{3+}$ is estimated to be 70 cm^{-1} by the Hush formula,[3] $H_{ab} = 0.0206(\varepsilon_{max}\nu_{max}\Delta\nu_{1/2})^{1/2}/(r_{ab})$, where the ET distance r_{ab} is estimated by the sum of two amine nitrogen−ruthenium distances (12.62 Å), the ε_{max} is 340 $M^{-1}cm^{-1}$ after subtracting the baseline, and the full width at the half height is 1100 cm^{-1}. However, this H_{ab} value is very likely underestimated due to the error in estimating the ET distance and the spectral deconvolution.

EPR Analysis of Aminium Radical Cations. The spin nature of the aminium radical cation $\mathbf{2}^{3+}$, obtained by chemical oxidation using $SbCl_5$, was probed by EPR analysis. Complex $\mathbf{2}^{3+}$ shows a three-line EPR signal at g = 2.0 at room temperature in CH_2Cl_2 (Figure 8). Similar signals have been reported for

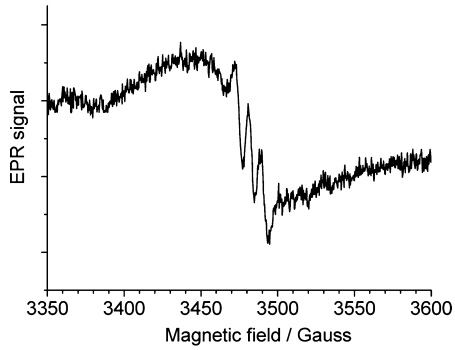

Figure 8. EPR signal of $\mathbf{2}^{3+}$ obtained by chemical oxidation using $SbCl_5$ in CH_2Cl_2 at room temperature.

aminium radical cations, as a result of the unpaired electron to a single ^{14}N nucleus.[22] This result strongly suggests that the unpaired electron is localized on the nitrogen atom, instead of the

DOI: 10.1021/ic5024967
Inorg. Chem. 2015, 54, 1272−1282

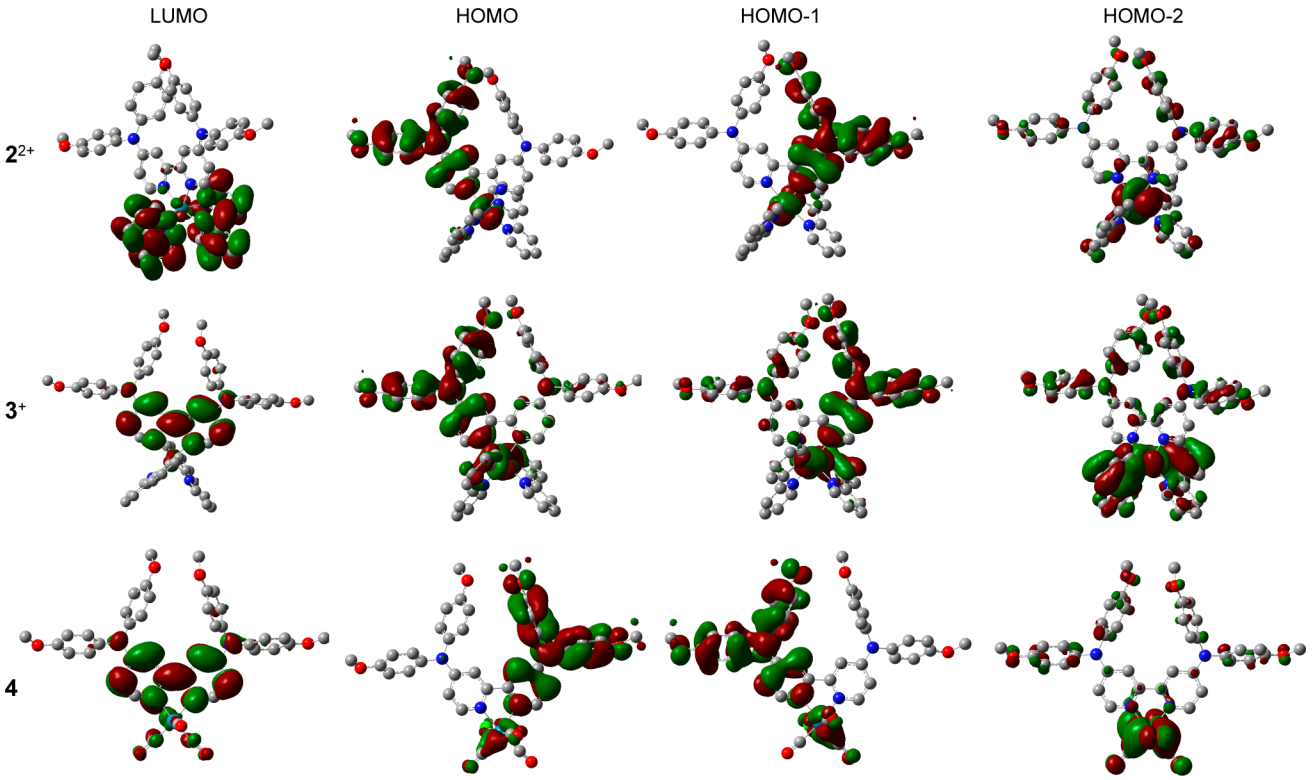

Figure 9. Selected frontier molecular orbitals of $\mathbf{2}^{2+}$–**4**.

ruthenium ion. Polypyridine ruthenium(III) complexes are well-known to be EPR inactive at room temperature due to fast spin relaxation by spin–orbital coupling.[23]

DFT and TDDFT Calculations. DFT calculations have been performed on $\mathbf{2}^{2+}$, $\mathbf{3}^{+}$, and **4** on the Gaussian 09 package.[24] The hybrid B3LYP exchange correlation functional[25] with the LANL2DZ basis set[26] for Ru, Ir, and Re, and 6-31G* for other atoms[27] were used. The computations were carried out taking into account solvation effects by means of the conductor polarizable continuum model (CPCM)[28] in CH_2Cl_2 solution. It has been found that the solvation has significant effects on the electronic structure and optical extinction energies of transition-metal complexes and MV compounds.[29]

Supporting Information Figure S2 shows the DFT-calculated frontier molecular orbital energy orderings of the above complexes. The predicted energy gaps between the highest occupied molecular orbital (HOMO) and the lowest unoccupied molecular orbital (LUMO) are 3.03, 3.35, and 3.49 eV for $\mathbf{2}^{2+}$, $\mathbf{3}^{+}$, and **4**, respectively. This trend is in agreement with the above electrochemical and spectroscopic studies.

The orbital compositions of HOMOs and LUMOs and other selected frontier orbitals of these complexes are shown in Figure 9 and Supporting Information Figure S3. The HOMO and HOMO − 1 orbitals of $\mathbf{2}^{2+}$, $\mathbf{3}^{+}$, and **4** are dominated by the triarylamine segment, with some involvement of the metal ion. The orbital overlap between the π orbitals of the triarylamine component and the dπ orbital of the metal ions can be observed for the HOMO and HOMO − 1 of all complexes. The HOMO − 2 orbitals of these complexes are mainly associated with the metal component, which are well-separated from the triarylamine orbitals. The LUMO and LUMO + 1 of $\mathbf{2}^{2+}$ are dominated by two bpy ligands, and its LUMO + 2 orbital has major contribution form the bpy unit of the NNbpy ligand. The LUMO orbitals of $\mathbf{3}^{+}$ and **4** are also dominated by the bpy unit of the NNbpy ligand.

To rationalize the absorption spectra of amine-containing ruthenium complexes, TDDFT calculations have been performed on $\mathbf{2}^{2+}$ (Figure S4 and Table S1, Supporting Information). The low-energy absorption tails around 520–600 nm are mainly associated with the S_3 and S_4 excitations, which can be interpreted as the LLCT transitions. The main absorption band in the visible region is associated with the S_5, S_6, S_7, S_8, and S_9 excitations, which contains multiple MLCT and ILCT transitions from the amine unit to the bpy unit.

On the basis of the optimized structure of $\mathbf{2}^{2+}$, DFT calculations have been performed on the singly oxidized forms, $\mathbf{2}^{3+}$, using the same level of theory (UB3LYP/LANL2DZ/6-31G*/CPCM). The calculated Mulliken spin density distribution is shown in Figure 10. The free spin of $\mathbf{2}^{3+}$ is predominantly localized within triarylamine segment, consistent with the above spectroscopic and EPR studies.

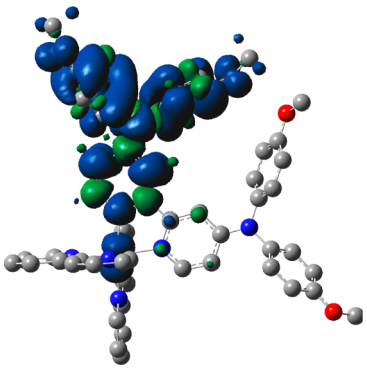

Figure 10. DFT-calculated spin-density distribution of $\mathbf{2}^{3+}$.

Table 3 and Figure 11 show the TDDFT results of the open-shell complex $\mathbf{2}^{3+}$. The IVCT transition, associated with the spin

DOI: 10.1021/ic5024967
Inorg. Chem. 2015, 54, 1272–1282

Table 3. TDDFT-Predicted Doublet (D) Excitations of 2^{3+} [a]

D_n	λ/nm	f	dominant transitions (percent contribution)
1	2493.1	0.0006	β-HOSO → β-LUSO (97%)
2	1415.3	0.0436	β-HOSO − 1 → β-LUSO (90%)
3	1205.5	0.0351	β-HOSO − 3 → β-LUSO (89%)
4	1159.7	0.0980	β-HOSO − 2 → β-LUSO (88%)
5	841.9	0.0005	β-HOSO − 4 → β-LUSO (98%)
6	816.9	0.2721	β-HOSO − 5 → β-LUSO (99%)

[a]Calculation method: UB3LYP/LANL2DZ/6-31G*/CPCM. The involved spin orbitals are displayed in Figure 11.

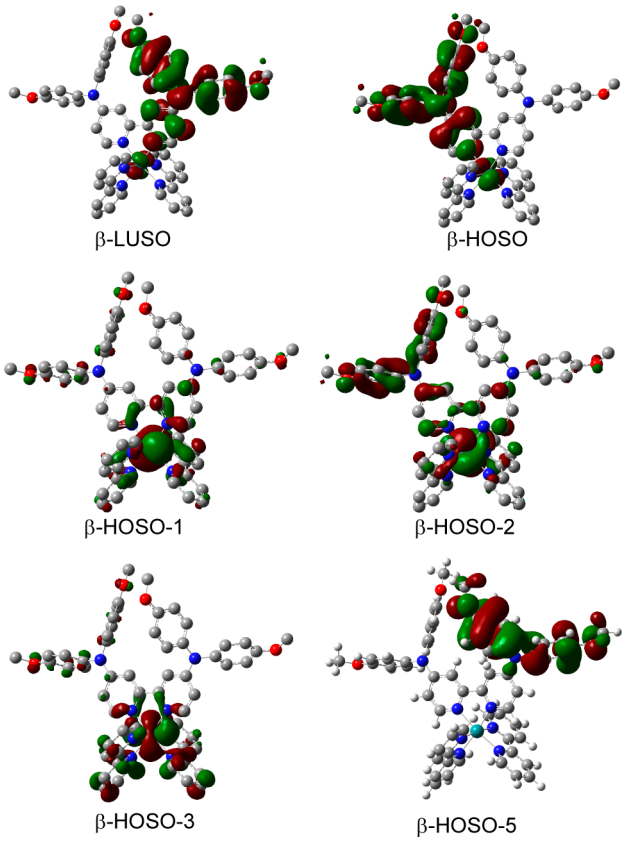

Figure 11. Frontier spin orbitals of 2^{3+} involved in the TDDFT results shown in Table 3.

transitions from the β-highest occupied spin orbital (HOSO) to the β-lowest unoccupied spin orbital (LUSO) (the D_1 excitation at 2493.1 nm), is predicted to locate in a low-energy region with weak oscillator strength (f = 0.0006). The ruthenium → aminium MLCT transitions have been well-reproduced by the TDDFT results with moderate strength (the D_2, D_3, and D_4 excitations). The $N^{\bullet+}$-localized transition is predicted by the D_6 excitation. Supporting Information Table S2 and Figures S5 and S6 show the TDDFT results of 3^{2+} and 4^{+}. IVCT transitions have been predicted for these two complexes at 2662.3 and 2278.7 nm, respectively. This is, however, inconsistent with the previous experimental findings, which reflect the limitation of TDDFT results for open-shell compounds.

Discussion on Electronic Coupling. The electrochemical and spectroscopic results consistently suggest that there is little amine−amine electronic coupling in NNbpy ligand. However, the coupling is enhanced by chelation with $Ru(bpy)_2$. It shows two stepwise amine oxidations with a potential splitting of 140 mV. The MV state of the resulting ruthenium complex displays a possible IVCT transition in the NIR region.

As has been discussed in the Introduction section, the two amine substituents on the chelated bpy ligand have close proximity, and there is a possibility for a through-space electronic coupling.[30] However, this possibility is low because no evidence has been observed to support the electronic coupling in the model Ir and Re complexes, where the two amine substituents have similar spatial orientations with those of the ruthenium complexes. This suggests that the amine−amine electronic coupling in 2^{3+} is more likely mediated by the ruthenium ion. DFT calculations show that the HOMO and HOMO − 1 orbitals of 2^{3+} are composed of the π orbitals of the triarylamine component and the dπ orbital of the ruthenium ion. This implies that the amine−amine electronic coupling mainly takes place via a hole-mediated superexchange mechanism, as has been proposed in most bistriarylamine MV systems. Namely, the electron transfer between $[N^{\bullet+}-Ru^{II}-N^0]$ and $[N^0-Ru^{II}-N^{\bullet+}]$ is mediated by a $[N^0-Ru^{III}-N^0]$ state.

The reason why the electronic coupling via the ruthenium bridge is larger with respect to that via the iridium or rhenium bridge is not clear at this stage. From a thermodynamic point of view, the Ir(IV) and Re(II) ions are equally accessible as Ru(III) for providing the hole transfer mediation, because Ir(III), Re(I), and Ru(II) ions can be oxidized at very similar potentials. One possible reason is that the Ru(II)−Ru(III) conversion can be faster with respect to the Ir(III)−Ir(IV) and Re(I)−Re(II) conversions. Supporting Information Figure S7 shows the DFT-calculated bond length changes of $[Ru(bpy)_3]^{2+}$, $[Ir(ppy)_2(bpy)]^{+}$, and $[Re(bpy)(CO)_3Cl]$ upon one-electron oxidation, which clearly shows that there is very little structural difference between $[Ru(bpy)_3]^{2+}$ and $[Ru(bpy)_3]^{3+}$. This would result in no significant reorganizational barrier to convert between $[N^{\bullet+}-Ru^{II}-N^0]$ and $[N^0-Ru^{III}-N^0]$ states and thus fast electron transfer kinetics and strong electronic coupling. However, much bigger structural changes are observed for $[Ir(ppy)_2(bpy)]^{+}$ and $[Re(bpy)(CO)_3Cl]$ upon one-electron oxidation. The little structural difference between $[Ru(bpy)_3]^{2+}$ and $[Ru(bpy)_3]^{3+}$ has previously been documented by comparing their single-crystal X-ray structures.[31] The big structural changes of rhenium bipyridine complexes upon oxidation can be seen from the time-resolved infrared spectroscopy upon photoexcitation.[32]

Another possibility to consider is that the $Ru(bpy)_2$ component has a charge of +2, while $Ir(ppy)_2$ has a charge of +1 and $Re(CO)_3Cl$ is neutral. The extra charge of $Ru(bpy)_2$ makes the MV state more stable (thus a larger potential splitting), allowing the IVCT to be observed. Although this possibility cannot be ruled out, such Coulombic effect is believed to be insignificant. This is supported by the facts that the potential splitting of the ruthenium complex observed with the weakly coordinating electrolyte $Bu_4NB(C_6F_5)_4$ only differs slightly with respect to that with Bu_4NClO_4 (155 versus 140 mV), and no sign of IVCT transitions appeared for the iridium complex in the presence of the $Bu_4NB(C_6F_5)_4$ electrolyte.

It is interesting to note that the positions of the amine substituents on bpy have a significant effect on the electronic coupling properties of the resulting ligand and metal complexes. We previously reported that the same two amine substituents display efficient electronic coupling through the 5,5′-positions of free bpy,[33] and this coupling can be slightly enhanced by metal chelation with $Ru(bpy)_2$, $Ir(ppy)_2$, and $Re(CO)_3Cl$. In the current study, we found there is no amine−amine coupling

DOI: 10.1021/ic5024967
Inorg. Chem. 2015, 54, 1272−1282

through the 4,4′-positions of free bpy, but the coupling can be enhanced by selective metal chelation with $Ru(bpy)_2$. This suggests that, in the previously reported 5,5′-NNbpy system, the bpy unit behaves the main and direct ET bridge, whose energy can be modulated by metal chelation. In the current 4,4′-NNbpy system, the ET is mediated by the orbital overlap between the pyridine ring and the ruthenium ion.

CONCLUSION

In summary, we have demonstrated that the amine−amine electronic coupling in the free 4,4′-NNbpy ligand has been enhanced by metal chelation. Interestingly, the metal species makes a big difference to this effect. Among three metal components studied [$Ru(bpy)_2$, $Ir(ppy)_2$, and $Re(CO)_3Cl$], only the chelation with $Ru(bpy)_2$ leads to the enhancement of the electronic coupling. This is supported by both the $N^{\bullet+/0}$ potential splitting and IVCT analysis. It is very likely that the amine−amine electron transfer in the ruthenium complex is mediated by the chelated ruthenium ion, instead of a through-space mechanism. This information is of high importance for the design of new mixed-valence systems and is useful for making molecular materials with switching functions.

EXPERIMENTAL SECTION

Spectroscopic Measurements. Absorption spectra were recorded on a PE Lambda 750 UV−vis−NIR spectrophotometer at room temperature. Spectroelectrochemical measurements were performed in a thin layer cell (optical length = 0.2 cm), in which an ITO glass electrode (<10Ω/square) working electrode was set in the indicated solvent containing the compound to be studied (concentration around 5×10^{-5} M) and 0.1 M Bu_4NClO_4 or $Bu_4NB(C_6F_5)_4$ as the supporting electrolyte. A platinum wire and Ag/AgCl in saturated aqueous NaCl was used as the counter electrode and reference electrode, respectively. The cell was put into the spectrometer to monitor the spectral change during electrolysis.

Electrochemical Measurement. All electrochemical measurements were taken using a CHI 660D potentiostat with one-compartment electrochemical cell under an atmosphere of nitrogen. All measurements were carried out in 0.1 M Bu_4NClO_4 or $Bu_4NB(C_6F_5)_4$ in indicated solvents at a scan rate of 100 mV/s. The working electrode was a glassy carbon with a diameter of 3 mm. The electrode was polished prior to use with 0.05 μm alumina and rinsed thoroughly with water and acetone. A large area platinum wire coil was used as the counter electrode. All potentials are referenced to a Ag/AgCl electrode in saturated aqueous NaCl without regard for the liquid junction potential. The potential versus ferrocene$^{+/0}$ can be subtracted by 0.45 V.

Computational Methods. DFT calculations are carried out using the B3LYP exchange correlation functional[25] and implemented in the *Gaussian* 09 package.[24] The electronic structures were optimized using a general basis set with the Los Alamos effective core potential LANL2DZ basis set for Ru, Ir, and Re,[26] and 6-31G* for other atoms.[27] The solvation effects are included for all calculations, and the conductor-like polarizable continuum model (CPCM) and united-atom Kohn−Sham (UAKS) radii were employed.[28] No symmetry constraints were used in the optimization (nosymm keyword was used). Frequency calculations have been performed with the same level of theory to ensure the optimized geometries to be local minima. All orbitals have been computed at an isovalue of 0.02 e/bohr^3.

Synthesis. NMR spectra were recorded in the designated solvent on Bruker Avance 400 MHz spectrometer. Spectra are reported in ppm values from residual protons of deuterated solvent. Mass data were obtained with a Bruker Daltonics Inc. Apex II FT-ICR or Autoflex III MALDI-TOF mass spectrometer. The matrix for MALDI-TOF measurement is α-cyano-4-hydroxycinnamic acid. Microanalysis was carried out using Flash EA 1112 or Carlo Erba 1106 analyzer at the Institute of Chemistry, Chinese Academy of Sciences. 4,4′-Dibromo-2,2′-bipyridine and 4-bromo-2,2′-bipyridine were prepared according to known procedures.[18] Electrolyte $Bu_4NB(C_6F_5)_4$ was prepared according to the Geiger's method.[34]

Synthesis of 1, NNbpy.[35] A suspension of 4,4′-dibromo-2,2′-bipyridine (100 mg, 0.32 mmol), bis(4-methoxyphenyl)amine (219 mg, 0.96 mmol), $Pd_2(dba)_3$ (29 mg, 0.032 mmol), dppf (18 mg, 0.032 mmol), and NaO^{t}Bu (92 mg, 0.96 mmol) in 10 mL toluene was heated at 140 °C for 48 h under a N_2 atmosphere. The system was cooled to room temperature. The solvent was removed under vacuum, and the crude product was purified by silica gel chromatography (eluting with 75:50:1 ethyl acetate/petroleum ether/$NH_3{\cdot}H_2O$) to yield 114 mg of **1** as a pale white solid in 59% yield. ^{1}H NMR (400 MHz, $CDCl_3$): δ 3.81 (s, 12H), 6.52−6.57 (m, 2H), 6.88 (d, J = 8.7 Hz, 8H), 7.13 (d, J = 8.7 Hz, 8H), 7.65 (s, 2H), 8.15 (d, J = 5.8 Hz, 2H). ^{13}C NMR (100 MHz, $CDCl_3$): δ 55.4, 108.8, 111.2, 115.0, 128.1, 138.4, 149.3, 155.1, 157.2, 157.5. EI-HRMS: calcd. 609.2509 for $C_{38}H_{34}N_4O_4$. Found: 610.2571. Anal. Calcd for $C_{38}H_{34}N_4O_4$: C, 74.73; H, 5.61; N, 9.17. Found: C, 74.74; H, 5.60; N, 9.15.

Synthesis of 2(PF$_6$)$_2$, [Ru(NNbpy)(bpy)$_2$](PF$_6$)$_2$. To a mixed solvent of 10 mL of ethanol and 5 mL of water were added **1** (36 mg, 0.060 mmol) and *cis*-$Ru(bpy)_2Cl_2{\cdot}2H_2O$ (37 mg, 0.080 mmol). The mixture was stirred and refluxed for 8 h under a N_2 atmosphere. After cooling to room temperature, ethanol was removed under reduced pressure, followed by the addition of an excess of aqueous KPF_6. The resulting precipitate was collected by filtering and washing with water and Et_2O. The obtained solid was subjected to flash column chromatography on silica gel (eluent: saturated aq $KNO_3/H_2O/CH_3CN$, 1/20/500), followed by anion exchange using KPF_6, to give 49 mg of **2**$(PF_6)_2$ as an orange solid in 62% yield. ^{1}H NMR (400 MHz, CD_3CN): δ 3.80 (s, 12H), 6.37 (d, J = 6.6 Hz, 2H), 6.94 (d, J = 8.7 Hz, 8H), 6.95 (overlapping, 2H), 7.00 (d, J = 6.6 Hz, 2H), 7.16 (d, J = 8.7 Hz, 8H), 7.28 (t, J = 6.6 Hz, 2H), 7.51 (t, J = 6.6 Hz, 2H), 7.67 (d, J = 5.5 Hz, 2H), 7.940−8.00 (m, overlapping, 4H), 8.06 (t, J = 8.1 Hz, 2H), 8.41 (d, J = 8.2 Hz, 2H), 8.46 (d, J = 8.1 Hz, 2H). ^{13}C NMR (100 MHz, CD_3CN): δ 55.9, 108.7, 112.9, 116.0, 124.6, 127.9, 128.0, 129.0, 136.7, 137.6, 137.7, 147.8, 150.7, 152.2, 152.3, 155.7, 157.0, 157.9, 158.1, 159.4. MALDI-MS: 1169.4 for $[M - PF_6]^+$, 1023.4 for $[M - 2PF_6]^+$, 864.1 for $[M - 2PF_6 - bpy]^+$. Anal. Calcd for $C_{58}H_{50}F_{12}N_8O_4P_2Ru$: C, 53.01; H, 3.84; N, 8.53. Found: C, 53.14; H, 3.85; N, 8.72.

Synthesis of 3(PF$_6$), [Ir(NNbpy)(ppy)$_2$](PF$_6$). To a mixed solvent of 10 mL of CH_2Cl_2 and 5 mL of MeOH was added **1** (50 mg, 0.082 mmol) and $[Ir(ppy)_2Cl]_2$ (44 mg, 0.041 mmol). The mixture was stirred and refluxed for 6 h under a N_2 atmosphere. After cooling to room temperature, an excess of aq KPF_6 was added. The suspension was stirred for 30 min and then filtered to remove insoluble inorganic salts. The filtrate was concentrated under reduced pressure to afford a crude yellow solid. The obtained solid was dissolved in 20 mL of CH_2Cl_2, followed by washing with H_2O (20 mL × 3). The organic phase was dried over anhydrous $MgSO_4$. The solvent was removed under reduced pressure, and the crude product was purified by silica gel chromatography (eluting with 100:1 CH_2Cl_2/MeOH) to give 86 mg **3**(PF_6) as a yellow solid in 83% yield. ^{1}H NMR (400 MHz, $CDCl_3$): δ 3.80 (s, 12H), 6.26 (d, J = 7.6 Hz, 2H), 6.41 (d, J = 6.4 Hz, 2H), 6.79 (t, J = 7.2 Hz, 2H), 6.87 (d, J = 8.0 Hz, 8H), 6.90 (overlapping, 2H), 6.99 (s, 2H), 7.16 (d, J = 7.6 Hz, 8H), 7.19 (s, 2H), 7.27 (d, overlapping, 2H), 7.58 (d, J = 8.0 Hz, 2H), 7.75 (t, J = 7.8 Hz, 2H), 7.81 (m, 4H). ^{13}C NMR (100 MHz, $CDCl_3$): δ 56.2, 109.2, 112.9, 116.0, 119.8, 122.5, 124.0, 125.1, 129.2, 131.0, 132.5, 136.5, 138.3, 144.5, 149.7, 149.9, 152.6, 156.0, 156.5, 159.2, 168.6. MALDI-MS: 1111.1 for $[M - PF_6]^+$. Anal. Calcd for $C_{60}H_{50}F_6N_6O_4PIr{\cdot}H_2O$: C, 56.55; H, 4.11; N, 6.60. Found: C, 56.44; H, 4.11; N, 6.49.

Synthesis of 4, [(NNbpy)Re(CO)$_3$Cl]. To 10 mL of dry toluene were added **1** (35 mg, 0.057 mmol) and $[Re(CO)_5Cl]$ (25 mg, 0.069 mmol). The mixture was stirred and refluxed for 8 h under a N_2 atmosphere. After cooling to room temperature, toluene was removed under reduced pressure. The obtained solid was subjected to flash column chromatography on silica gel (eluting with 40:1 CH_2Cl_2/ethyl acetate) to give 27 mg of complex **4** as an orange solid in 52% yield. ^{1}H NMR (400 MHz, $CDCl_3$): δ 3.84 (s, 12H), 6.55 (d, J = 6.4 Hz, 2H), 6.83 (s, 2H), 6.88 (d, J = 8.0 Hz, 8H), 7.10 (d, J = 8.0 Hz, 8H), 8.38 (s, 2H). ^{13}C NMR (100 MHz, $CDCl_3$): δ 56.2, 108.6, 112.5, 116.0, 128.9, 136.6, 153.0, 155.9, 156.8, 159.2, 192.2, 198.7. MALDI-MS: 881.1 for

DOI: 10.1021/ic5024967
Inorg. Chem. 2015, 54, 1272−1282

$[M - Cl]^+$. Anal. Calcd for $C_{41}H_{34}ClN_4O_7Re{\cdot}0.5H_2O$: C, 53.04; H, 4.13; N, 6.03. Found: C, 53.09; H, 3.74; N, 6.06.

Synthesis of 5, Nbpy. A suspension of 4-bromo-2,2′-bipyridine (100 mg, 0.43 mmol), bis(4-methoxyphenyl)amine (146 mg, 0.64 mmol), $Pd_2(dba)_3$ (20 mg, 0.020 mmol), dppf (12 mg, 0.020 mmol), and NaO^tBu (49 mg, 0.51 mmol) in 10 mL dry toluene was heated at 140 °C for 48 h under a N_2 atmosphere. The system was cooled to room temperature before the solvent was removed under vacuum. The crude product was purified by chromatography on silica gel (eluting with 25:15:1 petroleum ether/ethyl acetate/$NH_3{\cdot}H_2O$) to yield 131 mg of **5** as a yellow solid (80%). ^{1}H NMR (400 MHz, $CDCl_3$): δ 3.82 (s, 6H), 6.62 (d, J = 5.8 Hz, 1H), 6.91 (d, J = 8.8 Hz, 4H), 7.17 (d, J = 8.8 Hz, 4H), 7.23 (m, 1H), 7.75 (m, 2H), 8.27 (m, 2H), 8.56 (d, J = 4.8 Hz, 1H). ^{13}C NMR (100 MHz, $CDCl_3$): δ 56.8, 109.8, 112.7, 116.4, 122.5, 124.7, 129.5, 138.0, 139.6, 150.3, 150.9, 156.6, 158.0, 158.1, 158.7. EI-HRMS: calcd 383.1634 for $C_{24}H_{21}N_3O_2$. Found: 383.1638.

Synthesis of $6(PF_6)_2$, $[Ru(Nbpy)(bpy)_2](PF_6)_2$. To a mixed solvent of 10 mL of ethanol and 5 mL of water were added **5** (50 mg, 0.13 mmol) and $Ru(bpy)_2Cl_2{\cdot}2H_2O$ (82 mg, 0.16 mmol). The mixture was stirred and refluxed for 8 h under a N_2 atmosphere. After cooling to room temperature, ethanol was removed under reduced pressure, followed by the addition of an excess of aq KPF_6. The resulting precipitate was collected by filtering and washing with water and Et_2O. The obtained solid was subjected to flash column chromatography on silica gel (eluent: saturated aq $KNO_3/H_2O/CH_3CN$, 1/20/400), followed by anion exchange using KPF_6, to give 110 mg of complex $\mathbf{6}(PF_6)_2$ as an orange solid in 77% yield. ^{1}H NMR (400 MHz, CD_3CN): δ 3.81 (s, 6H), 6.45 (d, J = 6.8 Hz, 1H), 7.02 (d, J = 8.8 Hz, 4H), 7.05 (s, 1H), 7.26 (d, J = 8.8 Hz, 4H), 7.33 (m, 3H), 7.42 (t, J = 6.6 Hz, 1H),7.48 (m, 2H), 7.67 (t, J = 6.4 Hz, 2H), 7.71 (d, J = 5.6 Hz, 1H), 7.77 (d, J = 5.2 Hz, 1H), 7.87 (t, J = 8.0 Hz, 1H), 7.91 (d, J = 5.6 Hz, 1H), 8.03 (m, 5H), 8.46 (m, 4H). ^{13}C NMR (100 MHz, acetone-d_6): δ 49.1, 103.4, 107.1, 109.6 117.8, 118.4, 121.5 121.7 121.8, 122.7, 130.4, 131.7, 144.2, 145.7, 145.9, 149.5, 150.2, 151.3, 151.4, 151.6, 152.9. MALDI-MS: 942.2 for $[M - PF_6]^+$, 797.2 for $[M - 2PF_6]^+$, 639.6 for $[M - 2PF_6 - bpy]^+$. Anal. Calcd for $C_{44}H_{37}F_{12}N_7O_2P_2Ru$: C, 48.63; H, 3.43; N, 9.02. Found: C, 48.26; H, 3.56; N, 8.95.

■ ASSOCIATED CONTENT

Supporting Information

CV of $[Ru(bpy)_3](PF_6)_2$, DFT and TDDFT results, and NMR and mass spectra of new compounds. This material is available free of charge via the Internet at http://pubs.acs.org.

■ AUTHOR INFORMATION

Corresponding Author

*E-mail: zhongyuwu@iccas.ac.cn.

Notes

The authors declare no competing financial interest.

■ ACKNOWLEDGMENTS

We thank the National Natural Science Foundation of China (Grants 21271176, 91227104, 21472196, and 21221002), the National Basic Research 973 program of China (Grant 2011CB932301), the Ministry of Science and Technology of China (Grant 2012YQ120060), and the Strategic Priority Research Program of the Chinese Academy of Sciences (Grant XDB 12010400) for funding support.

■ REFERENCES

(1) Creutz, C.; Taube, H. *J. Am. Chem. Soc.* **1969**, *91*, 3988.

(2) (a) D'Alessandro, D. M.; Keene, F. R. *Chem. Rev.* **2006**, *106*, 2270. (b) Kaim, W.; Lahiri, G. K. *Angew. Chem., Int. Ed.* **2007**, *46*, 1778. (c) Aguirre-Etcheverry, P.; O'Hare, D. *Chem. Rev.* **2010**, *110*, 4839. (d) Low, P. J.; Brown, N. J. *J. Cluster Sci.* **2010**, *21*, 235. (e) Chisholm, M. H.; Lear, B. J. *Chem. Soc. Rev.* **2011**, *40*, 5254. (f) Liu, C. Y.; Xiao, X.; Meng, M.; Zhang, Y.; Han, M. J. *J. Phys. Chem. C* **2013**, *117*, 19859. (g) Xiao, X.; Meng, M.; Lei, H.; Liu, C. Y. *J. Phys. Chem. C* **2014**, *118*, 8308. (h) Ou, Y.-P.; Zhang, J.; Xu, M.; Xia, J.; Hartl, F.; Yin, J.; Yu, G.-A.; Liu, S. H. *Chem.—Asian J.* **2014**, *9*, 1152. (i) Das, H. S.; Schweinfurth, D.; Fiedler, J.; Khusniyarov, M. M.; Mobin, S. M.; Sarkar, B. *Chem.—Eur. J.* **2014**, *20*, 4334.

(3) (a) Hush, N. S. *Prog. Inorg. Chem.* **1967**, *8*, 391. (b) Hush, N. S. *Coord. Chem. Rev.* **1985**, *64*, 135.

(4) (a) Ward, M. D. *J. Solid State Electrochem.* **2005**, *9*, 778. (b) Kaim, W. *Coord. Chem. Rev.* **2011**, *255*, 2503. (c) Yao, C.-J.; Zhong, Y.-W.; Nie, H.-J.; Abruña, H. D.; Yao, J. *J. Am. Chem. Soc.* **2011**, *133*, 20720. (d) Yao, C.-J.; Yao, J.; Zhong, Y.-W. *Inorg. Chem.* **2012**, *51*, 6259. (e) Deibel, N.; Hohloch, S.; Sommer, M. G.; Schweinfurth, D.; Ehret, F.; Braunstein, P.; Sarkar, B. *Organometallics* **2013**, *32*, 7366.

(5) (a) Sporer, C.; Ratera, I.; Ruiz-Molina, D.; Zhao, Y.; Vidal-Gancedo, J.; Wurst, K.; Jaitner, P.; Clays, K.; Persoons, A.; Rovira, C.; Veciana, J. *Angew. Chem., Int. Ed.* **2004**, *43*, 5266. (b) Barnes, J. C.; Fahrenbach, A. C.; Dyar, S. M.; Frasconi, M.; Giesener, M. A.; Zhu, Z.; Liu, Z.; Hartlieb, K. J.; Carmieli, R.; Wasielewski, M. R.; Stoddart, J. F. *Proc. Natl. Acad. Sci. U.S.A.* **2012**, *109*, 11546.

(6) (a) Liu, I. P.-C.; Wang, W.-Z.; Peng, S.-M. *Chem. Commun.* **2009**, 4323. (b) Ying, J.-W.; Liu, I. P.-C.; Xi, B.; Song, Y.; Campana, C.; Zuo, J.-L.; Ren, T. *Angew. Chem., Int. Ed.* **2010**, *49*, 954. (c) Launay, J.-P. *Coord. Chem. Rev.* **2013**, *257*, 1544. (d) Sakamoto, R.; Katagiri, S.; Maeda, H.; Nishihara, H. *Coord. Chem. Rev.* **2013**, *257*, 1493. (e) Muratsugu, S.; Sodeyama, K.; Kitamura, F.; Sugimoto, M.; Tsuneyuki, S.; Miyashita, S.; Kato, T.; Nishihara, H. *J. Am. Chem. Soc.* **2009**, *131*, 1388. (f) Muratsugu, S.; Sodeyama, K.; Kitamura, F.; Tsukada, S.; Tada, M.; Tsuneyuki, S.; Nishihara, H. *Chem. Sci.* **2011**, *2*, 1960.

(7) (a) Simao, C.; Mas-Torrent, M.; Casado-Montenegro, J.; Oton, F.; Veciana, J.; Rovira, C. *J. Am. Chem. Soc.* **2011**, *133*, 13256. (b) Cui, B.-B.; Yao, C.-J.; Yao, J.; Zhong, Y.-W. *Chem. Sci.* **2014**, *5*, 932.

(8) (a) Li, Y.; Josowicz, M.; Tolbert, L. M. *J. Am. Chem. Soc.* **2010**, *132*, 10374. (b) Siebler, D.; Linseis, M.; Gasi, T.; Carrella, L. M.; Winter, R. F.; Forster, C.; Heinze, K. *Chem.—Eur. J.* **2011**, *17*, 4540. (c) Gonzalez, S. R.; Delgado, M. C. R.; Caballero, R.; De la Cruz, P.; Langa, F.; Navarrete, J. T. L.; Casado, J. *J. Am. Chem. Soc.* **2012**, *134*, 5675. (d) Wu, S.-H.; Shen, J.-J.; Yao, J.; Zhong, Y.-W. *Chem.—Asian J.* **2013**, *8*, 138. (e) Wu, S.-H.; Shao, J.-Y.; Kang, H.-W.; Yao, J.; Zhong, Y.-W. *Chem.—Asian J.* **2013**, *8*, 2843. (f) Hildebrandt, A.; Lang, H. *Organometallics* **2013**, *32*, 5640.

(9) (a) Olivier, C.; Costuas, K.; Choua, S.; Maurel, V.; Turek, P.; Saillard, J.-Y.; Touchard, D.; Rigaut, S. *J. Am. Chem. Soc.* **2010**, *132*, 5638. (b) Wadman, S. H.; Havenith, R. W. A.; Lutz, M.; Spek, A. L.; van Klink, G. P. M.; van Koten, G. *J. Am. Chem. Soc.* **2010**, *132*, 1914. (c) Wang, L.; Yang, W.-W.; Zheng, R.-H.; Shi, Q.; Zhong, Y.-W.; Yao, J. *Inorg. Chem.* **2011**, *50*, 7074. (d) Yao, C.-J.; Zhong, Y.-W.; Yao, J. *J. Am. Chem. Soc.* **2011**, *133*, 15697. (e) Xi, B.; Liu, I. P.-C.; Xu, G.-L.; Choudhuri, M. M. R.; DeRosa, M. C.; Crutchley, R. J.; Ren, T. *J. Am. Chem. Soc.* **2011**, *133*, 15094. (f) Glover, S. D.; Kubiak, C. P. *J. Am. Chem. Soc.* **2011**, *133*, 8721. (g) Linseis, M.; Zalis, S.; Zabel, M.; Winter, R. F. *J. Am. Chem. Soc.* **2012**, *134*, 16671. (h) Qu, Y.-P.; Xia, J.; Zhang, J.; Xu, M.; Yin, J.; Yu, G.-A.; Liu, S. H. *Chem.—Asian J.* **2013**, *8*, 2023. (i) Kobayashi, K.; Ishikubo, M.; Kanaizuka, K.; Kosuge, K.; Masaoka, S.; Sakai, K.; Nozaki, K.; Haga, M.-a. *Chem.—Eur. J.* **2011**, *17*, 6954.

(10) (a) Nelsen, S. E. *Chem.—Eur. J.* **2000**, *6*, 581. (b) Rosokha, S. V.; Kochi, J. K. *Acc. Chem. Res.* **2008**, *41*, 641. (c) Hankache, J.; Wenger, O. S. *Chem. Rev.* **2011**, *111*, 5138. (d) Heckmann, S.; Lambert, C. *Angew. Chem., Int. Ed.* **2012**, *51*, 326.

(11) (a) Johnson, R.; Hupp, J. T. *J. Am. Chem. Soc.* **2001**, *123*, 2053. (b) Nelsen, S. F.; Trieber, D. A., II; Ismagilov, R. F.; Teki, Y. *J. Am. Chem. Soc.* **2001**, *123*, 5684. (c) Nelsen, S. F.; Ismagilov, R. F.; Powell, D. R. *J. Am. Chem. Soc.* **1998**, *120*, 1924. (d) Nelsen, S. F.; Schultz, K. P. *J. Phys. Chem. A* **2009**, *113*, 5577.

(12) (a) Lambert, C.; Nöll, G. *J. Am. Chem. Soc.* **1999**, *121*, 8434. (b) Lambert, C.; Nöll, G.; Schelter, J. *Nat. Mater.* **2002**, *1*, 69. (c) Barlow, S.; Risko, C.; Chung, S.-J.; Tucker, N. M.; Coropceanu, V.; Jones, S. C.; Levi, Z.; Brédas, J.-L.; Marder, S. R. *J. Am. Chem. Soc.* **2005**, *127*, 16900. (d) Heckmann, A.; Amothor, S.; Lambert, C. *Chem. Commun.* **2006**, 2959. (e) Lacroix, J. C.; Chane-Ching, K. I.; Maquere,

DOI: 10.1021/ic5024967
Inorg. Chem. 2015, 54, 1272−1282

F.; Maurel, F. *J. Am. Chem. Soc.* **2006**, *128*, 7264. (f) Amothor, S.; Lambert, C. *J. Phys. Chem. A* **2006**, *110*, 1177. (g) Zhou, G.; Baumgarten, M.; Müllen, K. *J. Am. Chem. Soc.* **2007**, *129*, 12211. (h) Sakamoto, R.; Sasaki, T.; Honda, N.; Yamamura, T. *Chem. Commun.* **2009**, 5156. (i) Völker, S. F.; Renz, M.; Kaupp, M.; Lambert, C. *Chem.—Eur. J.* **2011**, *17*, 14147. (j) He, B.; Wenger, O. S. *J. Am. Chem. Soc.* **2011**, *133*, 17027. (k) Barlow, S.; Risko, C.; Odom, S. A.; Zheng, S.; Coropceanu, V.; Beverina, L.; Bredas, J.-L.; Marder, S. R. *J. Am. Chem. Soc.* **2012**, *134*, 10146.

(13) (a) Almlöf, J. E.; Feyereisen, M. W.; Jozefiak, T. H.; Miller, L. L. *J. Am. Chem. Soc.* **1990**, *112*, 1206. (b) Gautier, N.; Dumur, F.; Lloveras, V.; Vidal-Gancedo, J.; Veciana, J.; Rovira, C.; Hudhomme, P. *Angew. Chem., Int. Ed.* **2003**, *42*, 2765.

(14) (a) Lu, J.-M.; Rosokha, S. V.; Lindeman, S. V.; Neretin, I. S.; Kochi, J. K. *J. Am. Chem. Soc.* **2005**, *127*, 1797. (b) Nelsen, S. F.; Weaver, M. N.; Zink, J. I.; Telo, J. P. *J. Am. Chem. Soc.* **2005**, *127*, 10611. (c) Nelsen, S. F.; Weaver, M. N.; Telo, J. P. *J. Am. Chem. Soc.* **2007**, *129*, 7036. (d) Telo, J. P.; Jalilov, A. S.; Nelsel, S. F. *J. Phys. Chem. A* **2011**, *115*, 3016.

(15) (a) Jones, S. C.; Coropceanu, V.; Barlow, S.; Kinnibrugh, T.; Timofeeva, T.; Brédas, J.-L.; Marder, S. R. *J. Am. Chem. Soc.* **2004**, *126*, 11782. (b) Yao, C.-J.; Yao, J.; Zhong, Y.-W. *Inorg. Chem.* **2011**, *50*, 6847. (c) Yao, C.-J.; Zhong, Y.-W.; Yao, J. *Inorg. Chem.* **2013**, *52*, 4040. (d) Yao, C.-J.; Zheng, R.-H.; Nie, H.-J.; Cui, B.-B.; Shi, Q.; Yao, J.; Zhong, Y.-W. *Chem.—Eur. J.* **2013**, *19*, 12376. (e) Ramirez, C. L.; Pegoraro, C. N.; Filevich, O.; Bruttomeso, A.; Etchenique, R.; Parise, A. R. *Inorg. Chem.* **2012**, *51*, 1261. (f) Lambert, C.; Wagener, R.; Klein, J. H.; Grelaud, G.; Moos, M.; Schmiedel, A.; Holzapfel, M.; Bruhn, T. *Chem. Commun.* **2014**, *50*, 11350.

(16) (a) Pieslinger, G. E.; Albores, P.; Slep, L. D.; Baraldo, L. M. *Angew. Chem., Int. Ed.* **2014**, *53*, 1293. (b) Xu, G.-L.; Crutchley, R. J.; DeRosa, M. C.; Pan, Q.-J.; Zhang, H.-X.; Wang, X.; Ren, T. *J. Am. Chem. Soc.* **2005**, *127*, 13354. (c) Das, A. K.; Sarkar, B.; Fiedler, J.; Zalis, S.; Hartenbach, I.; Strobel, S.; Lahiri, G. K.; Kaim, W. *J. Am. Chem. Soc.* **2009**, *131*, 8895.

(17) (a) Sun, Y.; Wang, S. *Inorg. Chem.* **2009**, *48*, 3755. (b) Adugna, S.; Revunova, K.; Djukic, B.; Gorelsky, S. I.; Jenkins, H. A.; Lemaire, M. T. *Inorg. Chem.* **2010**, *49*, 10183. (c) Suzuki, H.; Kanbara, T.; Yamamoto, T. *Inorg. Chim. Acta* **2004**, *357*, 4335. (d) Li, H.-Y.; Cheng, L.-X.; Xiong, J.; Kang, L.-C.; Xu, Q.-L.; Zhu, Y.-C.; Tao, Y.-M.; Zheng, Y.-X.; Zuo, J.-L.; You, X.-Z. *Inorg. Chim. Acta* **2011**, *370*, 398. (e) Gao, Y.-T.; Zhang, H.; Jiang, T.; Yang, J.; Li, B.; Li, Z.; Hua, J.-L. *Sci. China Chem.* **2013**, *56*, 1204. (f) Zhang, Y.-M.; Wu, S.-H.; Yao, C.-J.; Nie, H.-J.; Zhong, Y.-W. *Inorg. Chem.* **2012**, *51*, 11387.

(18) (a) Staats, H.; Eggers, F.; Hab, O.; Fahrenkrug, F.; Matthey, J.; Lüning, U.; Lützen, A. *Eur. J. Org. Chem.* **2009**, 4777. (b) Carlson, B.; Phelan, G. D.; Kaminsky, W.; Dalton, L.; Jiang, X.; Liu, S.; Jen, A. K.-Y. *J. Am. Chem. Soc.* **2002**, *124*, 14162. (c) Bair, J. S.; Harrison, R. G. *J. Org. Chem.* **2007**, *72*, 6653. (d) Nie, H.-J.; Yao, J.; Zhong, Y.-W. *J. Org. Chem.* **2011**, *76*, 4771.

(19) (a) Handa, S.; Wietasch, H.; Thelakkat, M.; Durrant, J. R.; Haque, S. A. *Chem. Commun.* **2007**, 1725. (b) Robson, K. C. D.; Koivisto, B. D.; Gordon, T. J.; Baumgartner, T.; Berlinguette, C. P. *Inorg. Chem.* **2010**, *49*, 5335. (c) Robson, K. C. D.; Sporinova, B.; Koivisto, B. D.; Schott, E.; Brown, D. G.; Berlinguette, C. P. *Inorg. Chem.* **2011**, *50*, 6019. (d) Ji, Z.; Li, Y.; Pritchett, T. M.; Makarov, N. S.; Haley, J. E.; Li, Z.; Drobizhev, M.; Rebane, A.; Sun, W. *Chem.—Eur. J.* **2011**, *17*, 2479. (e) McClenaghan, N. D.; Passalacqua, R.; Loiseau, F.; Campagna, S.; Verheyde, B.; Hameurlaine, A.; Dehaen, W. *J. Am. Chem. Soc.* **2003**, *125*, 5356. (f) Liu, J.; Zhang, Q.; Ding, H.-J.; Zhang, J.; Tan, J.-Y.; Wang, C.-K.; Wu, J.-Y.; Li, S.-L.; Zhou, H.-P.; Yang, J.-X.; Tian, Y.-P. *Sci. China Chem.* **2013**, *56*, 1315. (g) Wang, Q.; Wu, W.; Ho, C.-L.; Xue, L.; Lin, Z.; Li, H.; Lo, Y. H.; Wong, W.-Y. *Eur. J. Inorg. Chem.* **2014**, 5322.

(20) (a) Matis, M.; Rapta, P.; Lukeš, V.; Hartmann, H.; Dunsch, L. *J. Phys. Chem. B* **2010**, *114*, 4451. (b) Reynolds, R.; Line, L. L.; Nelson, R. F. *J. Am. Chem. Soc.* **1974**, *96*, 1087. (c) Sreenath, K.; Thomas, T. G.; Gopidas, K. R. *Org. Lett.* **2011**, *13*, 1134. (d) Sreenath, K.; Suneesh, C. V.; Kumar, V. K. R.; Gopidas, K. R. *J. Org. Chem.* **2008**, *73*, 3245.

(21) (a) Ladouceur, S.; Zysman-Colman, E. *Eur. J. Inorg. Chem.* **2013**, 2985. (b) Baiano, J.; Carlson, D. L.; Wolosh, G. M.; DeJesus, D. E.; Knowles, C. F.; Szabo, E. G.; Murphy, W. R., Jr. *Inorg. Chem.* **1990**, *29*, 2327. (c) Wu, S.-H.; Abruna, H. D.; Zhong, Y.-W. *Organometallics* **2012**, *31*, 1161.

(22) (a) Lancaster, K.; Odom, S. A.; Jones, S. C.; Thayumanavan, S.; Marder, S. R.; Brédas, J.-L.; Coropceanu, V.; Barlow, S. *J. Am. Chem. Soc.* **2009**, *131*, 1717. (b) Kattnig, D. R.; Mladenova, B.; Grampp, G.; Kaiser, C.; Heckmann, A.; Lambert, C. *J. Phys. Chem. C* **2009**, *113*, 2983.

(23) Patra, S.; Sarkar, B.; Mobin, S. M.; Kaim, W.; Lahiri, G. K. *Inorg. Chem.* **2003**, *42*, 6469.

(24) Frisch, M. J.; Trucks, G. W.; Schlegel, H. B.; Scuseria, G. E.; Robb, M. A.; Cheeseman, J. R.; Montgomery, J. A.; Vreven, T., Jr.; Kudin, K. N.; Burant, J. C.; Millam, J. M.; Iyengar, S. S.; Tomasi, J.; Barone, V.; Mennucci, B.; Cossi, M.; Scalmani, G.; Rega, N.; Petersson, G. A.; Nakatsuji, H.; Hada, M.; Ehara, M.; Toyota, K.; Fukuda, R.; Hasegawa, J.; Ishida, M.; Nakajima, T.; Honda, Y.; Kitao, O.; Nakai, H.; Klene, M.; Li, X.; Knox, J. E.; Hratchian, H. P.; Cross, J. B.; Adamo, C.; Jaramillo, J.; Gomperts, R.; Stratmann, R. E.; Yazyev, O.; Austin, A. J.; Cammi, R.; Pomelli, C.; Ochterski, J. W.; Ayala, P. Y.; Morokuma, K.; Voth, G. A.; Salvador, P.; Dannenberg, J. J.; Zakrzewski, V. G.; Dapprich, S.; Daniels, A. D.; Strain, M. C.; Farkas, O.; Malick, D. K.; Rabuck, A. D.; Raghavachari, K.; Foresman, J. B.; Ortiz, J. V.; Cui, Q.; Baboul, A. G.; Clifford, S.; Cioslowski, J.; Stefanov, B. B.; Liu, G.; Liashenko, A.; Piskorz, P.; Komaromi, I.; Martin, R. L.; Fox, D. J.; Keith, T.; Al-Laham, M. A.; Peng, C. Y.; Nanayakkara, A.; Challacombe, M.; Gill, P. M. W.; Johnson, B.; Chen, W.; Wong, M. W.; Gonzalez, C.; Pople, J. A. *Gaussian 09, revision A.2*; Gaussian, Inc.: Wallingford, CT, 2009.

(25) Lee, C.; Yang, W.; Parr, R. G. *Phys. Rev. B* **1988**, *37*, 785.

(26) Hay, P. J.; Wadt, W. R. *J. Chem. Phys.* **1985**, *82*, 270.

(27) Dunning, T. H.; Hay, P. J. In *Modern Theoretical Chemistry*; Schaefer, H. F., Ed.; Plenum: New York, 1976; Vol. 3, p 1.

(28) (a) Barone, V.; Cossi, M. *J. Phys. Chem. A* **1998**, *102*, 1995. (b) Cossi, M.; Rega, N.; Scalmani, G.; Barone, V. *J. Comput. Chem.* **2003**, *24*, 669.

(29) (a) Fantacci, S.; De Angelis, F.; Selloni, A. *J. Am. Chem. Soc.* **2003**, *125*, 4381. (b) De Angelis, F.; Fantacci, S.; Selloni, A. *Chem. Phys. Lett.* **2004**, *389*, 204. (c) Fox, M. A.; Le Guennic, B.; Roberts, R. L.; Brue, D. A.; Yufit, D. S.; Howard, J. A. K.; Manca, G.; Halet, J.-F.; Hartl, F.; Low, P. J. *J. Am. Chem. Soc.* **2011**, *133*, 18433. (d) Costuas, K.; Rigaut, S. *Dalton Trans.* **2011**, *40*, 5643.

(30) (a) Sun, D.-L.; Rosokha, S. V.; Lindeman, S. V.; Kochi, J. K. *J. Am. Chem. Soc.* **2003**, *125*, 15950. (b) Casado, J.; Takimiya, K.; Otsubo, T.; Ramirez, F. J.; Quirante, J. J.; Ortiz, R. P.; Gonzalez, S. R.; Oliva, M. M.; Navarrete, J. T. L. *J. Am. Chem. Soc.* **2008**, *130*, 14028. (c) Cornelis, D.; Franz, E.; Asselberghs, I.; Clays, K.; Verbiest, T.; Koeckelberghs, G. *J. Am. Chem. Soc.* **2011**, *133*, 1317. (d) Jagtap, S. P.; Mukhopadhyay, S.; Coropceanum, V.; Brizius, G. L.; Bredas, J.-L.; Collard, D. M. *J. Am. Chem. Soc.* **2012**, *134*, 7176.

(31) Biner, M.; Burgi, H.-B.; Ludi, A.; Rohr, C. *J. Am. Chem. Soc.* **1992**, *114*, 5117.

(32) George, M. W.; Turner, J. J. *Coord. Chem. Rev.* **1998**, *177*, 201.

(33) Nie, H.-J.; Chen, X.; Yao, C.-J.; Zhong, Y.-W.; Hutchison, G. R.; Yao, J. *Chem.—Eur. J.* **2012**, *18*, 14497.

(34) (a) LeSuer, R. J.; Geiger, W. E. *Angew. Chem., Int. Ed.* **2000**, *39*, 248. (b) LeSuer, R.; Bettolph, C.; Geiger, W. E. *Anal. Chem.* **2004**, *76*, 6395.

(35) The synthesis and characterization of ligand **1** have recently been reported in ref 19g, where the carbon signal at 155.1 ppm is missing.

DOI: 10.1021/ic5024967
Inorg. Chem. 2015, 54, 1272−1282